Research Article | Vol. 8, No. 1 | 1 Jan 2018 | OPTICAL MATERIALS EXPRESS 82
Optical Materials EXPRESS

Fabrication of low-loss Rb-exchanged ridge waveguides in z-cut $KTiOPO_4$

MARTIN F. VOLK,[1,*] CHRISTIAN E. RÜTER,[1] MATTEO SANTANDREA,[2] CHRISTOF EIGNER,[2] LAURA PADBERG,[2] HARALD HERRMANN,[2] CHRISTINE SILBERHORN,[2] AND DETLEF KIP[1]

[1]*Faculty of Electrical Engineering, Helmut Schmidt University, 22043 Hamburg, Germany*
[2]*Department of Physics, University of Paderborn, 33098 Paderborn, Germany*
[*]*volk@hsu-hh.de*

Abstract: We report on the fabrication and characterization of ridge waveguides in z-cut $KTiOPO_4$ fabricated by Rb-ion exchange and subsequent precise diamond-blade dicing. Low attenuation values of 1.3 dB/cm (1.6 dB/cm) were determined at a wavelength of 1550 nm for TE (TM) polarization. Surface quality obtained by dicing is excellent for side walls of diced ridges and prepared end faces used for light coupling. The dispersion characteristics of the waveguides are determined and the results are compared to simulations. Finally, the nonlinear performance of the ridges is demonstrated by second harmonic generation of ~1060 nm pump light.

OCIS codes: (230.4000) Microstructure fabrication; (130.7405) Wavelength conversion devices; (230.7370) Waveguides.

References and links

1. J. D. Bierlein and H. Vanherzeele, "Potassium titanyl phosphate: properties and new applications," J. Opt. Soc. Am. B **6**(4), 622–633 (1989).
2. G. Qiu, H. T. Huang, B. T. Zhang, J. L. He, J. F. Yang, and J. L. Xu, "Highly efficient intracavity frequency doubling 532-nm laser based on the gray tracking resistance KTP crystal," Laser Phys. **20**(4), 777–780 (2010).
3. G. Harder, V. Ansari, B. Brecht, T. Dirmeier, C. Marquardt, and C. Silberhorn, "An optimized photon pair source for quantum circuits," Opt. Express **21**(12), 13975–13985 (2013).
4. F. König and F. N. C. Wong, "Extended phase matching of second-harmonic generation in periodically poled $KTiOPO_4$ with zero group-velocity mismatch," Appl. Phys. Lett. **84**(10), 1644–1646 (2004).
5. M. Rottschalk, J.-P. Ruske, B. Unterschütz, A. Rasch, and V. Gröber, "Single mode integrated-optical wide-band channel waveguides and junction splitters in $KTiOPO_4$ for visible light," J. Appl. Phys. **81**(6), 2504–2510 (1997).
6. S. Müller, T. Calmano, P. W. Metz, C. Kränkel, C. Canalias, C. Liljestrand, F. Laurell, and G. Huber, "Highly efficient continuous wave blue second-harmonic generation in fs-laser written periodically poled Rb:$KTiOPO_4$ waveguides," Opt. Lett. **39**(5), 1274–1277 (2014).
7. N. Dong, F. Chen, and J. R. Vazquez de Aldana, "Efficient second harmonic generation by birefringent phase matching in femtosecond-laser-inscribed KTP cladding waveguides," Phys. Stat. Sol. Rap. Res. Lett. **6**(7), 306–308 (2012).
8. Y. Tan, F. Chen, L. Wang, X.-L. Wang, K.-M. Wang, and Q.-M. Lu, "Optical channel waveguides in $KTiOPO_4$ crystal produced by proton implantation," J. Lightw. Technol. **26**(10), 1304-1308 (2008).
9. C. Chen, C. E. Rüter, M. F. Volk, C. Chen, Z. Shang, Q. Lu, S. Akhmadaliev, S. Zhou, F. Chen, and D. Kip, "Second harmonic generation of diamond-blade diced $KTiOPO_4$ ridge waveguides," Opt. Express **24**(15), 16434–16439 (2016).
10. M. F. Volk, S. Suntsov, C. E. Rüter, and D. Kip, "Low loss ridge waveguides in lithium niobate thin films by optical grade diamond blade dicing," Opt. Express **24**(2), 1386–1391 (2016).
11. Y. Jia, C. E. Rüter, S. Akhmadaliev, S. Zhou, F. Chen, and D. Kip, "Ridge waveguide lasers in Nd:YAG crystals produced by combining swift heavy ion irradiation and precise diamond blade dicing," Opt. Mater. Express **3**(4), 433–438 (2013).
12. S. Usenko, A. Przystawik, M. A. Jakob, L. L. Lazzarino, G. Brenner, S. Toleikis, C. Haunhorst, D. Kip, and T. Laarmann, "Attosecond interferometry with self-amplified spontaneous emission of a free-electron laser," Nature Commun. **8**, 15626 (2017).
13. M. F. Volk, C. E. Rüter, and D. Kip, "Rb/Ba side-diffused ridge waveguides in KTP," Opt. Express **25**(17), 19872–19877 (2017).
14. C. E. Rüter, J. Wisniewski, and D. Kip, "Prism coupling method to excite and analyze Floquet-Bloch modes in linear and nonlinear waveguide arrays," Opt. Lett. **31**(18), 2768–2770 (2006).
15. I. Shoji, T. Kondo, A. Kitamoto, M. Shirane, and R. Ito, "Absolute scale of second-order nonlinear-optical coefficients," J. Opt. Soc. Am. B **14**(9), 2268–2294 (1997).

#307766 https://doi.org/10.1364/OME.8.000082
Journal © 2018 Received 22 Sep 2017; revised 20 Nov 2017; accepted 26 Nov 2017; published 15 Dec 2017

Optical Materials EXPRESS

16. J. Vollmer, J. P. Nisius, P. Hertel, and E. Krätzig, "Refractive index profiles of $LiNbO_3$: Ti waveguides," Appl. Phys. A **32**(3), 125–127 (1983).

1. Introduction

Potassium titanyl phosphate (KTP, $KTiOPO_4$) is a nonlinear optical crystal that possesses high nonlinear optical coefficients, wide transparency range, good thermal stability and high optical damage threshold [1]; it has found widespread application in nonlinear optics. For example, KTP is frequently used for frequency-doubling (SHG) of solid state laser radiation [2]; in quantum information applications KTP is also a very attractive candidate for generating entangled photon pairs using spontaneous parametric down conversion (SPDC), because it allows for narrow photon bandwidths and high heralding efficiencies [3]. To fully exploit the nonlinear properties of KTP, though, it is usually necessary to tailor the phasematching properties of the crystal through periodic poling, which is possible mainly in z-cut KTP crystals [4].

Compared to both bulk samples and planar waveguides, the use of two-dimensional (2D) waveguides in KTP enables higher efficiencies in frequency conversion and allows for integration with other optical components on the same substrate [5]. The most widespread method for channel waveguide fabrication is ion exchange of K ions through Rb ions in a nitrate salt melt through a photolithographically patterned mask [1]. Also other methods, such as fs-laser writing [6, 7] or ion implantation [8, 9] have been successfully used for the fabrication of 2D waveguides in KTP. However, either high losses or poor mode coupling are limiting factors of such waveguides. As an alternative method, precise diamond-blade dicing of crystalline materials allows for direct preparation of optical-grade surfaces and thus has attracted increased interest for fabrication of e.g. ridge waveguide structures [10], waveguide lasers [11] or XUV beam splitters [12].

Recently, we fabricated ridge waveguides by a side-exchange method in x-cut KTP [13] that possess high resistance against higher temperature and allow for stronger mode confinement and higher overlap between modes of different wavelength, compared to conventional waveguides in KTP. However, a drawback of x-cut ridge waveguides is that they cannot be periodicaly poled using established methods. Such periodic poling is inevitable for many applications to achieve the required quasi-phasematching (QPM). Therefore, in the work presented here, we fabricated ridge waveguides in z-cut KTP crystals by a combination of Rb-ion exchange and ridge definition by a diamond-blade dicing saw. In this way most of the advantages of ridge waveguides are preserved, in particular the improved mode overlap of waves of different wavelengths. By optimization of the dicing parameters we are able to fabricate single mode ridge waveguides with very low surface roughness and low optical losses. An analysis of the waveguide dispersion is performed by measurement of effective mode indices and comparison with simulation results.

2. Experiments

We fabricated planar waveguides in commercial flux-grown KTP crystals by ion exchange in a Rb nitrate ($RbNO_3$) bath at 370 °C for 1 h. Subsequent ridge definition was performed with a diamond-blade dicing saw [9, 13], as shown in Fig. 1(a). These ridges were cut into the +z face parallel to the x-axis. Before cutting the above mentioned sample several blades were evaluated on a KTP test substrate. Following the nomenclature of Disco Corp., the following three blades (A,B,C) showed best results: P1A863 SD6000 N100 BR16 (A), P1A863 SD6000 N100 BR50 (B) and G1A853 SD6000 R21B01 (C). All blades are 100 μm wide, have the finest grit available (i. e. typical particle size of 2 μm), but differ in the particle density and bond composition. Figure 2 shows confocal microscope images of 20 μm deep grooves in a test substrate using the different blades at two feed rates. We notice that a lower feed rate results in less fracture and that blades B and C cause hardly any chipping at 0.5 μm/rev. As the wear and thus the rounding of blade C was smaller than that of B, blade C was chosen for preparing the ridges in the final sample. The two

Optical Materials EXPRESS

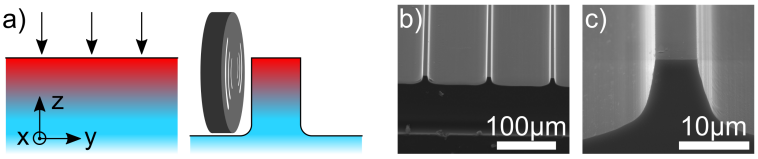

Fig. 1. a) Waveguides are formed in the +z face of KTP by Rb in-diffusion and subsequent ridge definition. b) and c) SEM images of completed ridge waveguides.

edges of each groove are shown as the two sides regularly differ in quality, with the side facing the spindle and blade mount having less fracture (see Fig. 2, blades A,B,C at 1 µm/rev).

Electron microscope (SEM) images of completed ridge waveguides are presented in Figs. 1(b,c), showing sharp edges and smooth surfaces. Using a white light interferometer, we measured a side-wall roughness of 1-2 nm. We prepared ridges of widths between 5 µm and 12 µm and heights between 10 µm and 20 µm. The width of the slightly trapezoid waveguide cross section (angles are ~ 85°) was determined at a depth of 5 µm measured from top of the ridge to deliver an effective value close to the center of a guided optical mode.

The fabricated waveguides have a gradient-index profile into the depth and thus differ from the side-exchange ridges with rectangular waveguide cross section achieved in [13]. However, they still profit from the large index-step in lateral direction. In order to compare with experimental results in the following, simulations were performed assuming an error-function shaped index profile $\Delta n(z) = \Delta n_0[1 - \mathrm{erf}(z/d)]$ with an exchange depth of $d = 10$ µm and an index increase of $\Delta n_0 = 14 \cdot 10^{-3}$ at the surface. This exchange depth has been determined (with an accuracy up to ±0.4 µm) by energy-dispersive x-ray spectroscopy (EDX) measurements of the Rb concentration with an electron beam microscope. On the other hand, the index increase was estimated numerically to account for the narrowest waveguide that was experimentally guiding (5.3 µm) at 1550 nm. Moreover, for simplicity the index increase was assumed independent of polarization and wavelength.

To investigate the guiding properties of the waveguides we first used a SM-fiber coupled laser at 1550 nm. Mode images of a 11.3 µm wide ridge waveguide are shown in Fig. 3(a) for TE and TM polarization and are compared to simulated ones. The overlap of waveguide modes, corresponding to ridges of different widths, with the SM fiber was calculated from these mode images and is displayed in Fig. 3(b), along with simulated curves. For a waveguide width of 11.3 µm the overlap is ~90%, which is close to the calculated value. For smaller ridges (that go along with narrower modes) it decreases to 60% for a ~5 µm wide ridge. Mode size and overlap were found to be independent of the cutting depth (i. e. ridge height). This is reasonable as the cutting depth was as deep as or deeper than the exchange depth for all ridges.

Using the cut-back method for a sample of initial length 8.4 mm (cut to two pieces of lengths

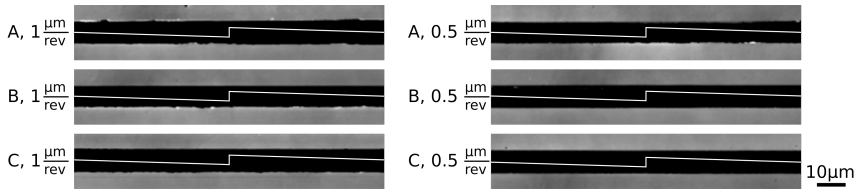

Fig. 2. Confocal microscope images of grooves prepared in the +z face of a KTP substrate using three different resin-based blades (A,B,C) at two different feed rates. Only the top of the substrate is shown and the center of the groove is omitted (white line). The upper edges face the blade-mount and spindle.

Optical Materials EXPRESS

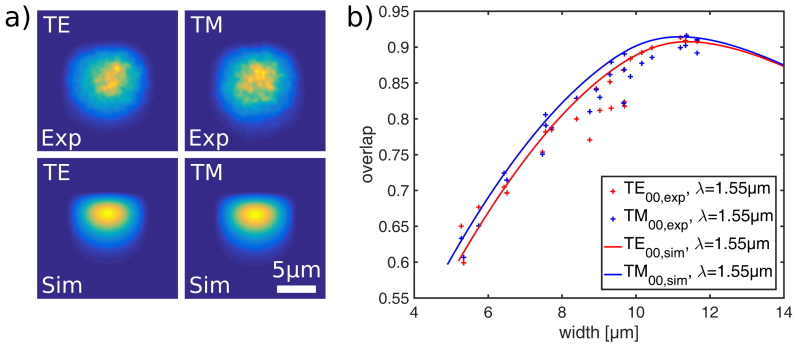

Fig. 3. a) Mode images (intensity) of a 11.3 µm wide waveguide and corresponding simulated modes at 1550 nm; b) spatial overlap between modes of optical SM fiber and ridge waveguides at 1550 nm, calculated from mode images and simulation.

6.9 mm/1.4 mm) and inspecting ridges of width larger than 9.5 µm, we measured attenuation of 1.3 dB/cm (1.6 dB/cm) for TE (TM) polarization. The measured total insertion loss can be as low as 2.6 dB for both polarizations. Although being comparable with channel waveguides formed in KTP, these propagation losses are slightly higher than the very low losses reported recently for x-cut ridges [13]. We attribute the increased losses to a higher brittleness of the waveguides, which makes them more prone to microfracture during dicing. This arises from the higher Rb concentration in the waveguide, as a consequence of the different exchange conditions (higher temperature and higher Rb concentration in the melt).

Due to the differences introduced by the waveguide geometry to the bulk dispersion properties, it is essential to have a precise knowledge of the waveguide dispersion, in order to determine the crystal orientation for critical phasematching, as well as to calculate the required grating period of periodically-poled KTP ridge waveguides. In order to investigate waveguide dispersion, we coupled light of 532 nm wavelength into the ridge waveguides by prism coupling and imaged the mode through a microscope objective onto a camera. Here a slight tilt of the impinging laser beam is needed to allow for the excitation of higher order modes [14]. The results of the measurements of effective indices are presented in Figs. 4(a,b) and are compared to simulations. We have to note that the experimentally determined differences in the refractive indices between the modes

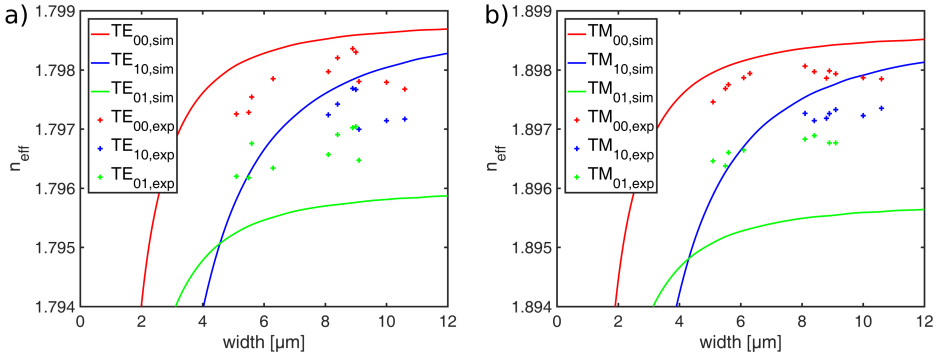

Fig. 4. Experimentally determined effective indices (symbols) of ridge waveguides of different width and simulation results (solid lines) for a) TE and b) TM polarization at 532 nm.

Optical Materials EXPRESS

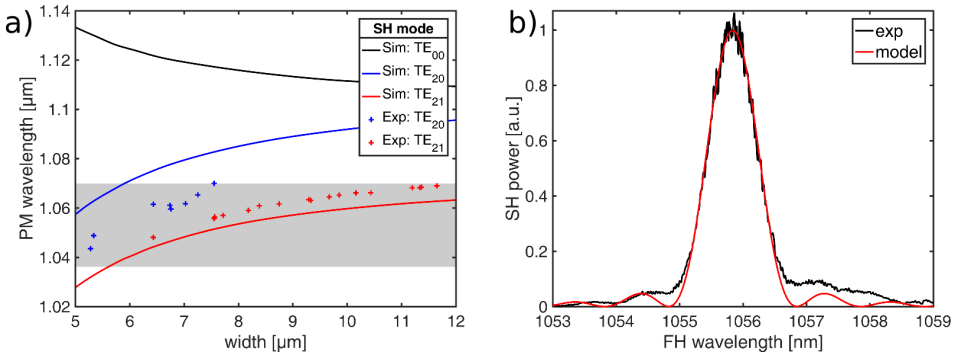

Fig. 5. a) Experimental and simulated phasematching wavelength of type-II SHG from fundamental TE_{00} and TM_{00} of ~1060 nm to higher order SH modes for ridges of different width; the grey area indicates the tuning range of the laser; b) measured (black) and calculated (red) phasematching curve of a 7.6 µm wide and 6.6 mm long ridge waveguide for conversion to TE_{21}; the calculated curve's width is that of bulk KTP and it's center was fitted to the experiment.

are assumed to be quite accurate, since they depend only on the precision in the measurement of angular differences. On the other hand, the absolute value of the refractive index is less precise, since its estimation is based on precise knowledge of the coupling prism's angle and refractive index; for this reason, it had to be matched to the simulated curves.

The sample under examination was an unpoled sample; for this reason, it is not possible to examine the nonlinear properties at 1550 nm, and we are limited to study the birefringent properties of the sample. Therefore, using SHG and type II phasematching, we coupled light from a fiber-coupled tunable amplifier system (Sacher Serval Plus) in the wavelength range of (1036 - 1070) nm polarized at an angle of 45 ° relative to the z-axis into the ridges. Within this tuning range we observed phasematching from the excited TE_{00}/TM_{00} fundamental pump modes to TE_{20}, TE_{21} and other higher-order SH modes. Conversion towards the fundamental TE_{00} mode was not found, and we expect it at a wavelength of ~1150 nm, outside the laser's tuning range (see Fig. 5(a)). Although the waveguides are partially multimode at the pump wavelength of ~1060 nm, the mode of the fundamental harmonic can be clearly excited when observing the SH signal while slightly shifting the in-coupling fiber. Figure 5(a) shows the experimental phasematching wavelength as a function of ridge widths, along with simulated curves. An experimental phasematching curve of a ridge waveguide is shown in Fig. 5(b). The original measurement showed Fabry-Perot oscillations and was smoothed for better visibility. The measured spectral bandwidth for the 6.6 mm long sample was 0.88 nm, corresponding to a bandwidth-length product of 0.58 nm·cm, close to the theoretical value of 0.59 nm·cm for bulk KTP. This indicates that the waveguide's width and exchange profile remain constant along the length of the waveguide. As an example, some experimental SH modes are displayed in Fig. 6, opposed to simulated ones.

Highest conversion efficiency of $\eta_{exp} = 0.17\,\%/(\mathrm{W\,cm^2})$ was found for a 5.3 µm wide ridge of length $L = 6.6$ mm at phasematching toward the TE_{20} mode at a pump wavelength of 1043.5 nm and a pump power of 230 mW (maximum power of the laser at stated wavelength). This efficiency is quite low; however, this is well understandable because of the poor overlap of the pump wave with a higher-order SH mode. We calculated the overlap integral S by integrating the scalar amplitude of the electric field distributions E_{FH} and E_{SH} obtained from mode images. The sign of the electric field amplitude of the SH mode was adjusted for the lobes manually. The obtained

Optical Materials EXPRESS

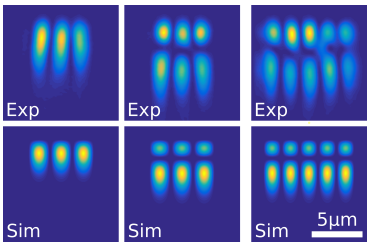

Fig. 6. Experimental and simulated SH modes of a 6.5 µm (left, middle) and a 9.0 µm wide (right) ridge waveguide.

value of $S = 0.045\,\mu\text{m}^{-1}$ was used to calculate a theoretically expected efficiency of

$$\eta_{\text{theo}} = \frac{P_{\text{SH}}}{P_{\text{FH}}^2 L^2} = \frac{8\pi^2 d_{24}^2 S^2}{n^3 c \epsilon_0 \lambda_{\text{FH}}^2} = 0.35\,\%/(\text{Wcm}^2). \quad (1)$$

Here $n = 1.79$ and $d_{24} = 1.9\,\text{pm/V}$ were used [15]. The deviation by a factor of ~2 between experimental and theoretical efficiency is expected to be caused partially by waveguide losses, which arise especially for the higher order SH modes, and eventually by inaccuracy of the mode overlap calculation. From simulations we find an overlap between pure fundamental modes (i. e. conversion towards TE_{00}) of $S_{\text{opt}} = 0.32\,\mu\text{m}^{-1}$; the corresponding conversion efficiency would thus be about 17.7 %/(W cm^2) when losses are neglected.

Comparing the earlier mentioned model for the simulations with the experimental results we find certain disagreement. In Figs. 4(a,b) the difference in refractive index between the experimental modes is approximately only half the simulated value. This indicates that the exchange depth of the model should be assumed larger. Assuming larger exchange depth also lowers the difference between the phasematching wavelength of different SH modes in Fig. 5(a). Furthermore, a deeper exchange profile in the model enlarges the depth of the simulated modes in Fig. 6, making them more comparable to the experimental ones. This suggests that the exchange depth of the optical index increase differs from that of the Rb concentration. A possible explanation could be that the Rb concentration profile and the refractive index change are related by a power law with an exponent smaller than one, as it was found for the refractive index changes induced by Ti in lithium niobate [16].

3. Conclusions

In conclusion, by use of a diamond-blade dicing saw and Rb exchange, we have successfully fabricated ridge waveguides in z-cut KTP with low surface roughness that allow for relatively low losses. Such z-cut ridge waveguides, when additionally periodically poled using existing methods, are good candidates for highly-efficient nonlinear frequency conversion devices and allow for a wider application range than the recently fabricated side-exchanged waveguides in x-cut KTP, where periodic poling could be very challenging. When compared to waveguides fabricated using ion implantation, no complicated equipment like high-energy accelerators is required, and much smaller widths can be obtained. We have shown that waveguide dispersion can be measured for the fabricated ridge waveguides with good accuracy. In future work, our results may be used for the fabrication of QPM ridge waveguides in z-cut KTP for nonlinear frequency conversion.